


 Very Important Paper

# Coherent Evolution of Signal Amplification by Reversible Exchange in Two Alternating Fields (alt-SABRE)

 Andrey N. Pravdivtsev,<sup>\*,[a]</sup> Nicolas Kempf,<sup>[b]</sup> Markus Plaumann,<sup>[c]</sup> Johannes Bernarding,<sup>[c]</sup> Klaus Scheffler,<sup>[b]</sup> Jan-Bernd Hövener,<sup>[a]</sup> and Kai Buckenmaier<sup>\*,[b]</sup>

Parahydrogen (pH<sub>2</sub>) is a convenient and cost-efficient source of spin order to enhance the magnetic resonance signal. Previous work showed that transient interaction of pH<sub>2</sub> with a metal organic complex in a signal amplification by reversible exchange (SABRE) experiment enabled more than 10% polarization for some <sup>15</sup>N molecules. Here, we analyzed a variant of SABRE, consisting of a magnetic field alternating between a low field of ~1 μT, where polarization transfer is expected to take place, and a higher field > 50 μT (alt-SABRE). These magnetic fields affected the amplitude and frequency of polarization transfer. Deviation of a lower magnetic field from a "perfect" condition of level anti-crossing increases the frequency of polarization transfer that can be exploited for polarization of short-lived transient SABRE complexes. Moreover, the coherences responsible for polarization transfer at a lower field persisted during magnetic field variation and continued their spin evolution at higher field with a frequency of 2.5 kHz at 54 μT. The latter should be taken into consideration for an efficient alt-SABRE. Theoretical and experimental findings were exemplified with Iridium N-heterocyclic carbene SABRE complex and <sup>15</sup>N-acetonitrole, where a 30% higher <sup>15</sup>N polarization with alt-SABRE compared to common SABRE was reached.

The amplification of nuclear spin polarization or hyperpolarization has enabled many exciting applications in chemistry,<sup>[1,2]</sup> catalysis,<sup>[3]</sup> biology<sup>[4]</sup> and, in particular, medical diagnostics.<sup>[5,6]</sup>

For the latter, the major challenge is a relatively short lifetime of the enhancement (typically < 1 minute)<sup>[7]</sup> and a one-time administration of hyperpolarized media (bolus) to the object of interest.<sup>[6,8]</sup> Although continuous polarization was demonstrated,<sup>[9–12]</sup> it does not have yet a medical application, as e.g. an alternative to computed tomography angiography where rapid and multiple injections of contrast are needed. Therefore, the goal remains to polarize a given sample to the maximum, and the quest for such methods is ongoing.

Parahydrogen (pH<sub>2</sub>) based techniques provide one of the most cost-efficient<sup>[13]</sup> ways to enhance the MR signal with <sup>13</sup>C polarization over 50%<sup>[14]</sup> and <sup>15</sup>N polarization over 20%.<sup>[15]</sup> pH<sub>2</sub> is a spin-isomer of molecular hydrogen whose nuclear spins are in the singlet spin state  $|S\rangle = (|\alpha\beta\rangle - |\beta\alpha\rangle)/\sqrt{2}$  with  $\alpha$  and  $\beta$  being spin states with parallel and anti-parallel projections of spin-1/2.

Signal amplification by reversible exchange (SABRE)<sup>[16]</sup> of pH<sub>2</sub> with a substrate, S, allows to convert the para-order into observable polarization continuously and within seconds. SABRE is a dynamic process and polarization transfer occurs only in the transient Ir-pH<sub>2</sub>-S complex. Still the contact time of pH<sub>2</sub> and S, or lifetime of such Ir-complex,  $\tau_i$ , is sufficiently long to allow polarization transfer by free evolution<sup>[16]</sup> or RF-pulses.<sup>[17]</sup> The most efficient "spontaneous" polarization transfers in the static magnetic field in SABRE happens at or near a level anti-crossing (LAC) magnetic field  $B_{LAC}$ .<sup>[18]</sup> It was shown that the increase of temperature or the exchange rates (or decrease of  $\tau_i$ ) results in broadening of the magnetic field region<sup>[19]</sup> of effective polarization transfer and moves its maximum up-field.<sup>[15]</sup> At a LAC or near  $B_{LAC}$ , the singlet state of pH<sub>2</sub> couples with its triplet states such that the polarization is distributed between the crossed states.<sup>[20]</sup> For <sup>1</sup>H-SABRE,  $B_{LAC}$  is on the order of 6 mT (LAC of pH<sub>2</sub> and <sup>1</sup>H of substrate), while fields on the order of 1 μT are needed to transfer spin order from pH<sub>2</sub> to <sup>15</sup>N.<sup>[21]</sup> The latter experiment was dubbed SABRE in SShield Enables Alignment Transfer to Heteronuclei (SABRE-SHEATH).<sup>[21]</sup>

Recently it was shown that fast and repetitive alternation (1–50 Hz) between  $B_{low} \sim 1 \mu T$  and a field in the range of  $50 \mu T < B_{high} < 100 \mu T$  (alt-SABRE-SHEATH, Figure 1a) depicts the J-coupling-driven coherent polarization transfer at  $B_{low}$ .<sup>[22]</sup> This method also provides even higher polarization than SABRE-SHEATH at constant field (Figure 1b).<sup>[22]</sup> Here, we report our observations on tweaking alt-SABRE-SHEATH towards shorter dwell times  $t_{high}$  at  $B_{high}$  so that the spin evolution at  $B_{high}$  also effects the polarization transfer.

In SABRE, polarization transfer takes place in the active SABRE complex like [IrH<sub>2</sub>S<sub>2</sub>] (Figure 2a, SI section 1), which

[a] Dr. A. N. Pravdivtsev, Prof. Dr. J.-B. Hövener  
Molecular Imaging North Competence Center (MOIN CC),  
Section Biomedical Imaging, Department of Radiology and Neuroradiology,  
University Medical Center Kiel, Kiel University  
Am Botanischen Garten 14, 24114 Kiel, Germany  
E-mail: andrey.pravdivtsev@rad.uni-kiel.de

[b] N. Kempf, Prof. Dr. K. Scheffler, Dr. K. Buckenmaier  
High-Field Magnetic Resonance Center,  
Max Planck Institute for Biological Cybernetics  
Max-Planck-Ring 11, 72076 Tübingen, Germany  
E-mail: kai.buckenmaier@tuebingen.mpg.de

[c] Dr. M. Plaumann, Prof. Dr. Dr. J. Bernarding  
Institute for Biometrics and Medical Informatics,  
Otto-von-Guericke University  
Building 02, Leipziger Str. 44, 39120 Magdeburg, Germany

 Supporting information for this article is available on the WWW under <https://doi.org/10.1002/cphc.202100543>

 © 2021 The Authors. ChemPhysChem published by Wiley-VCH GmbH. This is an open access article under the terms of the Creative Commons Attribution Non-Commercial License, which permits use, distribution and reproduction in any medium, provided the original work is properly cited and is not used for commercial purposes.

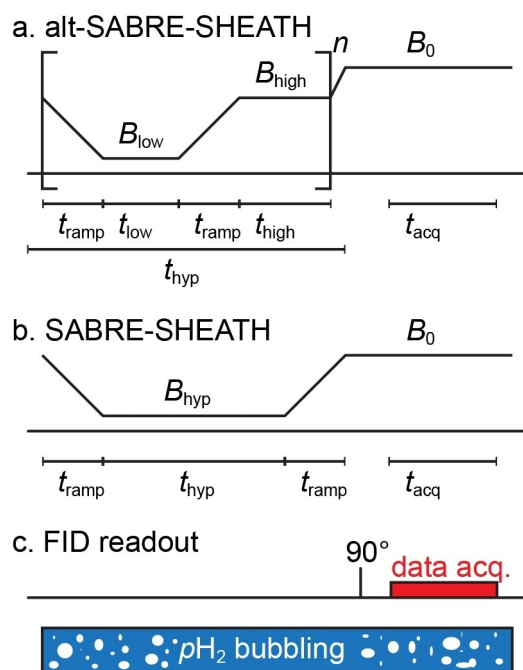


**Figure 1. Sequence schematics.** (a) Magnetic field pattern for alt-SABRE-SHEATH and (b) for SABRE-SHEATH. (c) A simple free induction decay (FID) readout consisting of a pulse excitation of  $^1\text{H}$  and  $^{15}\text{N}$  spins ( $B_1$ ) and signal acquisition at  $B_0 \approx 54 \mu\text{T}$  with duration  $t_{\text{acq}}$ . Alt-SABRE-SHEATH consists of a hyperpolarization stage of length  $t_{\text{hyp}}$ , where the magnetic field is alternated between  $B_{\text{low}}$  and  $B_{\text{high}}$  with duration  $t_{\text{low}}$  and  $t_{\text{high}}$  respectively. This part is repeated  $n$  times (total hyperpolarization time  $t_{\text{hyp}}$ ). In our experiments, the hyperpolarization stage is followed by a simple FID readout. During the entire experiment  $\text{pH}_2$  is continuously supplied with a flow rate of  $\approx 2.5 \text{ L/h}$  for convenience. Susceptibility effects on magnetic field homogeneity are negligible that is demonstrated by a spectral linewidth  $< 0.5 \text{ Hz}$  at  $B_0 \approx 54 \mu\text{T}$ .

comprises an Ir-complex with ligands,  $\text{H}_2$  and two equatorial substrates  $S$ .<sup>[23]</sup> The chemical kinetics between  $S$  and  $[\text{IrH}_2\text{S}_2]$  can be approximated using a dissociation rate constant  $k_d$  and pseudo-first-order association rate constant  $k'_a$ .<sup>[19,24,25]</sup> The theoretical findings illustrated in Figure 2 were validated experimentally using  $^{15}\text{N}$ -acetonitrile as a substrate and  $[\text{IrImesCODCl}]$ <sup>[23]</sup> as a precursor of active SABRE complex with  $\text{Imes} = 1,3$ -bis(2,4,6-trimethylphenyl) imidazole-2-ylidene and  $\text{COD} = 1,5$ -cyclooctadiene in methanol- $\text{H}_4$ . We expect that the method also works for other SABRE-active substrates.<sup>[26]</sup> The SABRE complex was activated as described before.<sup>[26,27]</sup>

For the sake of simplicity, the spin system of  $[\text{IrH}_2\text{S}_2]$  can be simplified to an  $\text{AA}'\text{XX}'$  type 4-spin system:  $\text{AA}'$  are the protons from  $\text{pH}_2$  and  $\text{XX}'$  are the  $^{15}\text{N}$  nuclei of the equatorial substrates. The  $\text{AA}'$  as well as the  $\text{XX}'$  system can be described using the singlet-triplet basis:  $|S\rangle, |T_-\rangle = |\beta\beta\rangle, |T_0\rangle = (|\alpha\beta\rangle + |\beta\alpha\rangle)/\sqrt{2}, |T_+\rangle = |\alpha\alpha\rangle$ . Subsequently, the spin state of the complete system can be described with a ket vector  $|KM\rangle$  where  $K$  stands for the  $\text{AA}'$  states and  $M$  for the  $\text{XX}'$  part.

Below  $1 \mu\text{T}$  there is a LAC between two states:  $|SS\rangle$  and  $|T_-\text{T}_+\rangle$  with an energy level splitting on the order of  $|^2J_{\text{HN}}^{\text{trans}} - ^2J_{\text{HN}}^{\text{cis}}|$ , where  $^2J_{\text{HN}}^{\text{trans}}$  describes the  $J$ -coupling constant for opposite  $^1\text{H}$  and  $^{15}\text{N}$  and  $^2J_{\text{HN}}^{\text{cis}}$  for neighboring nuclei.<sup>[21]</sup> This is

the one pair of coupled spin states that is responsible for SABRE-SHEATH polarization transfer from  $\text{pH}_2$  to  $^{15}\text{N}$ . The  $|SS\rangle$  state is overpopulated when fresh  $\text{pH}_2$  binds to  $[\text{Ir}]$ , and the interaction between crossing states  $|SS\rangle$  and  $|T_-\text{T}_+\rangle$  results in a maximum SABRE-SHEATH polarization at a LAC (Figure 2b). In fact, because  $|J_{\text{HH}}| \approx 8 \text{ Hz} < |^2J_{\text{HN}}^{\text{trans}} - ^2J_{\text{HN}}^{\text{cis}}| \approx 24 \text{ Hz}$  the LAC for SABRE-SHEATH (SI, Figure S9) is not as defined as in the case of  $^1\text{H}$ -SABRE.<sup>[18,27]</sup> The analytical expressions for LACs in 3 spin systems consisting of two protons and one X-nucleus were obtained by Eills et al.<sup>[28]</sup>

Other energy states (and coherences) are also populated when  $\text{pH}_2$  is added and affect the spin order transfer. It is important that the total spin projection of the states is constant (e.g. 0 for  $|SS\rangle$  and  $|T_-\text{T}_+\rangle$  states) because scalar spin-spin interaction cannot change the total projection of the state. This means that zero-quantum coherences (or transitions) transfer spin order in this case.

When the magnetic field is higher or lower than  $B_{\text{LAC}}$ , the mixing efficiency of the crossing states decreases while the rate of polarization transfer increases (or decreases) since there is no complete match of the Zeeman interaction and  $J$ -coupling constants. alt-SABRE SHEATH reproduces this LAC analysis (Figure 2c).

The coherently driven polarization transfer from  $\text{pH}_2$  to  $S$  near  $B_{\text{LAC}}$  with a frequency on the order of the scalar spin-spin coupling constants (Figure 2c) was already experimentally verified by Lindale et al. for relatively long  $\text{pH}_2$  refreshing times  $t_{\text{high}} > 200 \text{ ms}$  at  $B_{\text{high}} = 55 \mu\text{T}$ .<sup>[22]</sup> When  $t_{\text{high}} \gg \tau_l$  (Figure 2c, left), all substrates and  $\text{pH}_2$  will exchange with the one in solution and  $[\text{Ir}]$  with refreshed  $\text{pH}_2$  is ready for the next cycle of polarization transfer at  $B_{\text{low}}$ . This effect can be well reproduced using a SABRE model based on either Markov chain Monte Carlo simulations of chemical exchange,<sup>[22,24]</sup> infinite-order perturbation approach<sup>[29]</sup> or the modified Liouville von Neumann equation with chemical exchange superoperators used here (Figure 2).<sup>[19,24]</sup>

Interestingly, if  $B_{\text{low}} \ll B_{\text{high}}$  and the magnetic field variation is short (for simplicity we assume each interval is fast:  $t_{\text{low}}, t_{\text{high}}, t_{\text{ramp}} \leq \tau_l = 1/k_d = 50 \text{ ms}$ ) then the  $^1\text{H}$ - $^{15}\text{N}$  zero-quantum coherences ( $^1\text{H}$ - $^{15}\text{N}$ -ZQ) created at  $B_{\text{low}}$  are retained and continue to evolve at  $B_{\text{high}}$  at an elevated frequency of  $(\gamma_{^1\text{H}} B_{\text{high}} - \gamma_{^{15}\text{N}} B_{\text{high}}) / 2\pi = \nu_{^1\text{H}} + |\nu_{^{15}\text{N}}|$  (Figure 2d). Here,  $\gamma_x$  is the magnetogyric ratio and  $\nu_x$  is the corresponding Larmor frequency with  $X = ^1\text{H}$  or  $^{15}\text{N}$ . Note that  $\gamma_{^{15}\text{N}}$  is negative, so, the resulting frequency of the polarization oscillations is higher than  $\nu_{^1\text{H}}$ . Here,  $^1\text{H}$ - $^{15}\text{N}$ -ZQs are spin orders that involve two spins: one  $^1\text{H}$  of hydride protons of  $[\text{Ir}]$  and one  $^{15}\text{N}$  of bound substrate. Their chemical dissociation results in a collapse of the wave function, meaning that the population of this spin order will be lost. This effect is illustrated on Figure 2c (right plot), where the oscillation amplitude decreases for long  $t_{\text{low}}$ .

Note the difference between the two cases of alt-SABRE-SHEATH illustrated in Figure 2c and 2d. When  $t_{\text{low}} \sim 1/J_{\text{NH}}$  (Figure 2c), the polarization transfer primarily happens at  $B_{\text{low}}$ . However, if  $t_{\text{low}} \ll 1/J_{\text{NH}}$ , the polarization transfer still can happen, but at  $B_{\text{high}}$  (Figure 2d). In this case, it will be additionally modulated by Zeeman interactions. In both regimes, alt-SABRE-

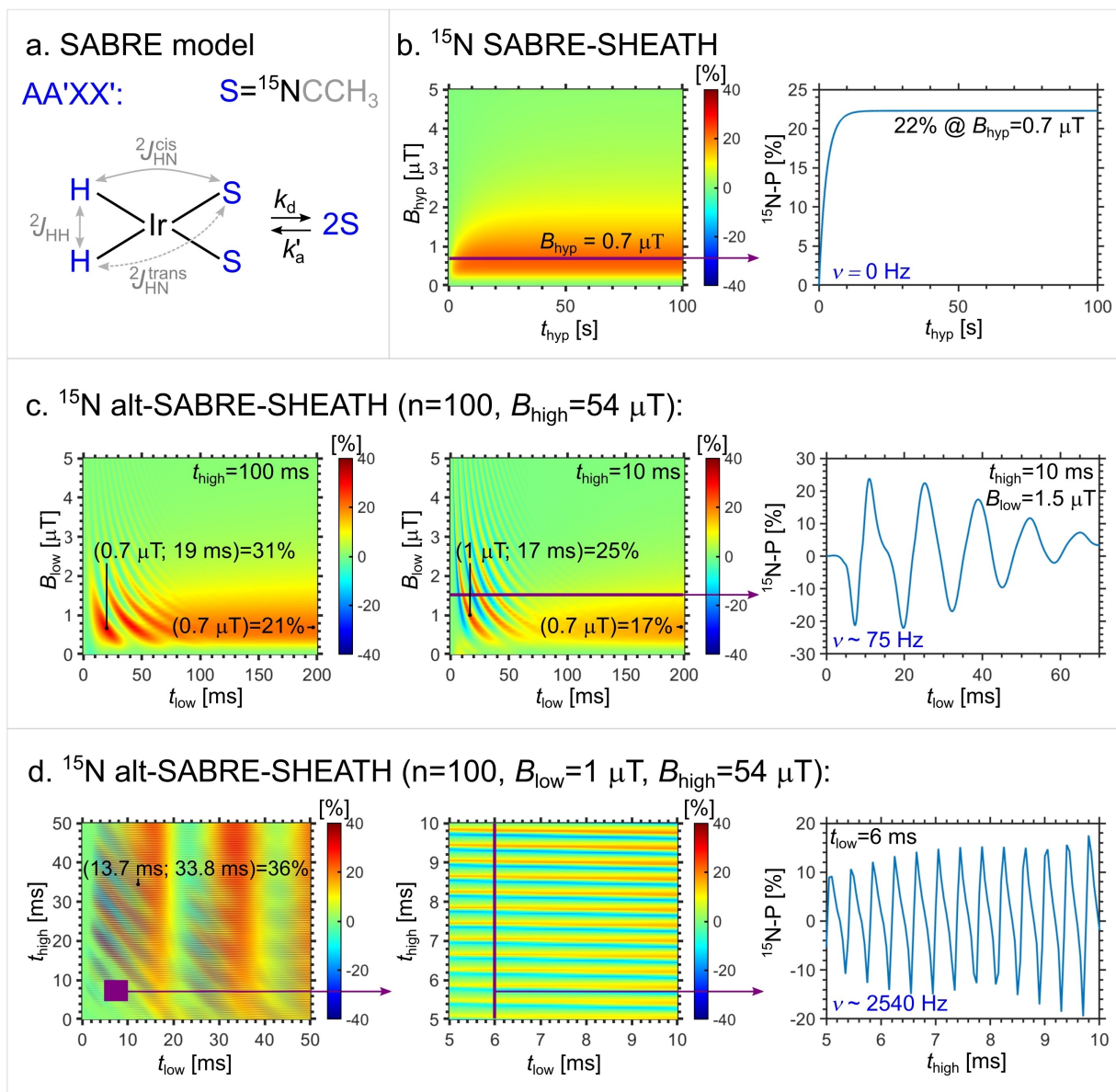


**Figure 2.** Simulations of (alt-)SABRE-SHEATH experiments. (a) AA'XX' system and SABRE exchange model.<sup>[19,24]</sup> (b)  $^{15}\text{N}$  SABRE-SHEATH (Figure 1a) polarization as a function of magnetic field  $B_{\text{hyp}}$ , hyperpolarization time  $t_{\text{hyp}}$  and polarization build-up at  $B_{\text{hyp}} = 0.7 \mu\text{T}$ . (c)  $^{15}\text{N}$  alt-SABRE-SHEATH (Figure 1b) polarization of S as a function of  $B_{\text{low}}$  and  $t_{\text{low}}$  for  $t_{\text{high}} = 100 \text{ ms}$  and  $t_{\text{low}} = 10 \text{ ms}$  and an example of polarization oscillations. (d)  $^{15}\text{N}$  alt-SABRE-SHEATH polarization of S as a function of  $t_{\text{low}}$  and  $t_{\text{high}}$  for  $B_{\text{low}} = 1 \mu\text{T}$  and  $B_{\text{high}} = 54 \mu\text{T}$ . When both time periods are short the faster oscillations are visible (oscillation frequencies  $\nu$  are given for the example kinetics – right plots).  $B_{\text{low}} = 1 \mu\text{T}$  in (d) is an example, experimentally alt-SABRE-SHEATH at several fields was measured (SI, Figure S5–S7). System parameters used for simulations were<sup>[19,24]</sup>  $k_a' = 2 \text{ s}^{-1}$ ,  $k_d = 20 \text{ s}^{-1}$ ,  $t_{\text{ramp}} = 0$ ,  $n = 100$ ; the complex consisted of two protons and two  $^{15}\text{N}$  with a high field  $T_1$  of 1 s and 6 s, chemical shifts are  $-22 \text{ ppm}$  and  $0 \text{ ppm}$  and  $^2J_{\text{HN}}^{\text{trans}} = -24 \text{ Hz}$ ,  $^2J_{\text{HN}}^{\text{cis}} = 0$  and  $^2J_{\text{HH}} = -8 \text{ Hz}$ ; after dissociation of  $^{15}\text{N}$  its high-field  $T_1$  was 60 s and chemical shift 100 ppm. Two substrates S in the Ir-complex were considered; each consisted of one  $^{15}\text{N}$ . Note the change of the frequency of polarization transfer in (c). Three purple lines on (b), (c), and (d) indicate the cut plane for the graphs on the right. One purple box in (d, left) describes the sector which is expanded in the middle graph.

SHEATH provides significantly higher polarization levels of the free substrate than SABRE-SHEATH (simulations, Figure 2b vs. 2c,d).

For experimental validation, we used a SQUID-based ultra-low field (ULF) NMR spectrometer (SI, Figure S10),<sup>[30]</sup> allowing the simultaneous observation of all MR visible nuclei (in our case  $^1\text{H}$  and  $^{15}\text{N}$ ). Although the chemical shift resolution is missing due to ULF detection at  $B_0 = 54 \mu\text{T}$ , the field homoge-

neity of the setup is sufficient to obtain  $J$ -resolved NMR spectra with a linewidth  $< 0.5 \text{ Hz}$  during constant  $\text{pH}_2$  bubbling (Figure 1).

The setup was proved to be very robust for long lasting SABRE experiments, which was demonstrated through ULF-SABRE-correlation spectroscopy (COSY) lasting more than 8 hours straight at room temperature and pressure with continuous  $\text{pH}_2$  supply.<sup>[31]</sup> After mixing  $[\text{Ir}(\text{Mes})\text{CODCI}]$ ,  $^{15}\text{N}$ -

acetonitrile in methanol- $H_4$  and flushing  $pH_2$  for 5 minutes at atmospheric pressure, the SABRE complex was activated, which followed from constant polarization produced in SABRE-SHEATH experiment (SI, Figure S3).

In a common SABRE-SHEATH experiment, the system was flushed with  $pH_2$  at a given field  $B_{hyp}$  for a time period  $t_{hyp}$  and then shuttled to the observation field (Figure 1a).<sup>[21]</sup> In our case, we simply increased  $B_{hyp}$  after polarization to reach  $B_0 \sim 54 \mu T$  for ULF NMR observation. The maximum polarization was achieved at  $1.2 \mu T$  (SI, Figure S2).

In the next step, the slow alt-SABRE-SHEATH oscillations near  $B_{low} = 1 \mu T$  were demonstrated for different  $t_{high}$  and  $B_{low}$  (Figure 3). The amplitude of  $^{15}N$  (Figure 3a) and  $^1H$  signals was found to oscillate as function of  $t_{high}$  as expected (Figure 3b). Figure 3c shows the integrated real part,  $ReI$ , of the  $^{15}N$  spectrum, complemented with a sinusoidal fit of the polarization oscillation frequency  $\nu$ .

The lowest  $\nu \sim 70$  Hz was near  $B_{LAC} \sim 1.2 \mu T$  (SI, Figure S4c) and increased to  $\nu \sim 119$  Hz at  $\sim 2.6 \mu T$  (Figure 3c and SI, Figure S5c) and  $\nu \sim 185$  Hz at  $\sim 3.9 \mu T$  (SI, Figure S6c). In the case of short-lived SABRE complexes,  $\nu$  is equivalent to the rate of polarization transfer, meaning higher  $\nu$  can achieve higher signal gain, despite the fact, that  $B_{low}$  is not fulfilling the optimum  $B_{LAC}$  condition.

Next, we kept both  $t_{low}$  and  $t_{high}$  shorter than  $1/J_{HN}$ . These settings resulted in an observation of a much faster oscillation with a frequency close to  $\nu_{1H} + |\nu_{15N}|$  as function of  $t_{high}$  (Figure 2d and Figure 4). As discussed above, the frequency is equal to the  $^1H-^{15}N$  two-spin order zero quantum coherence at

$B_0$ . And, as expected, both  $^{15}N$  (Figure 4a and 4c) and  $^1H$  signals (Figure 4b) showed these oscillations. This fast oscillation was observed for different parameter settings (SI, Figure S7 and S8). Due to the long hyperpolarization build up times ( $> 10$  s) and limited availability of the involved substances (acetonitrile, Ir-catalyst), only a very narrow parameter space of the performed simulations could be experimentally assessed. However, these results confirm that although the polarization is generated at low fields, the evolution continues at high fields, where only refreshment of the Ir-complex was assumed. Here, we show that the length of  $t_{high}$  is also important for alt-SABRE-SHEATH hyperpolarization.

Interestingly, that with alt-SABRE-SHEATH spin order oscillates between  $^1H$  and  $^{15}N$  of acetonitrile (Figure 3 and 4), thus increasing the signal intensity for this specific nucleus. The importance of multiple quantum coherences for SABRE experiments was already shown in Ref. [31], where the COSY spectrum of a hyperpolarized spin system with multiple orders was predicted and experimentally verified. It was shown that for a conventional SABRE experiment, the spin-order of  $pH_2$  distributes among all coupled spins: their magnetization and various  $zz$ -spin orders were found to be populated.

We were able to probe the fast spin dynamics of the active SABRE complex and achieved a 30% higher  $^{15}N$  polarization with alt-SABRE-SHEATH compared to common SABRE-SHEATH of equal  $t_{hyp}$  (SI, section 8), in accordance with the theory. This was accomplished using the sequence parameters depicted in Figure 4.

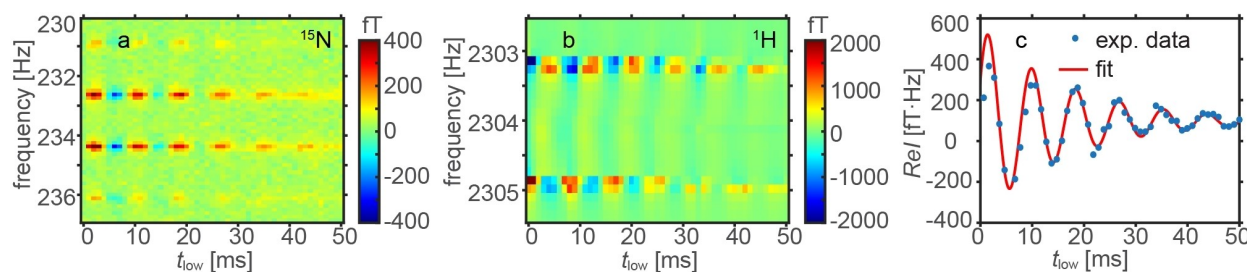


**Figure 3.** Experimental alt-SABRE-SHEATH  $^{15}N$  and  $^1H$  spectra (a, b) and integral over the real part of the  $^{15}N$  signal (c) as a function of  $t_{low}$  at  $B_{low} = 2.6 \mu T$ . Note that both  $^{15}N$  and  $^1H$  signals of acetonitrile oscillate as a function of  $t_{low}$  (these protons are neglected in the simulations). Other experimental parameters:  $t_{hyp} = 30$  s,  $t_{high} = 10$  ms, and  $B_{high}$ ,  $B_0 = 54 \mu T$ . The kinetics (c) were fitted by  $f = A + B(2\pi\nu t_{low} + \phi)e^{-t_{low}/T_d}$  (fit, line) with fitting parameters:  $\nu = 119.0 \pm 1.1$  Hz and  $T_d = 17.0 \pm 2.1$  ms.

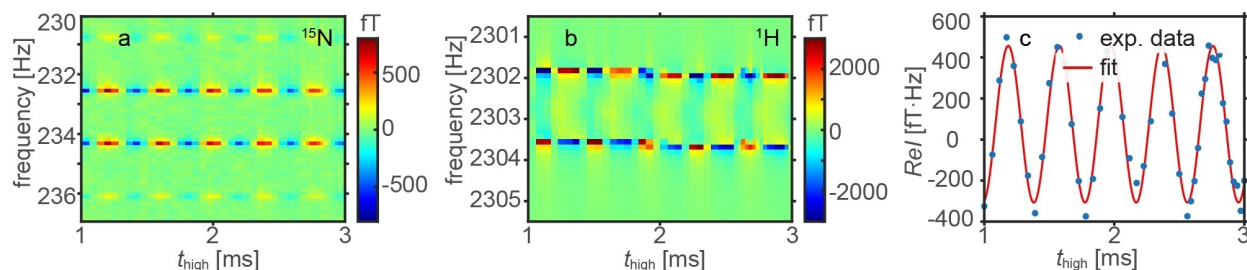


**Figure 4.** Experimental alt-SABRE-SHEATH  $^{15}N$  and  $^1H$  spectra (a, b) and integral over the real part of the  $^{15}N$  spectrum (c) as a function of  $t_{high}$  at  $B_{high} = 54 \mu T$ . Note that both  $^{15}N$  and  $^1H$  signals of acetonitrile oscillate as a function of  $t_{high}$  (these protons are neglected in the simulations). Other experimental parameters:  $B_{low} = 2.6 \mu T$ ,  $t_{hyp} = 30$  s,  $t_{low} = 1.5$  ms, and  $B_0 = 54 \mu T$ . The kinetics (c) were fitted by  $f = A + B(2\pi\nu t_{high} + \phi)$  (fit, line) with fitting parameters:  $\nu = 2541 \pm 13$  Hz.

The analysis of alt-SABRE performance showed that instead of non-adiabatic (fast in respect to LAC frequency splitting) variation of external magnetic fields, slower ramps maybe beneficial, which will prevent such a fast and detrimental oscillation at  $B_{\text{high}}$ . Moreover, adiabatic passages through the LAC condition were reported to be beneficial for polarization transfer.<sup>[32,33]</sup>

In parallel with this work, it was suggested to replace the  $(t_{\text{high}}, B_{\text{high}})$  block with two blocks:  $(t_{\text{high}/2}, B_{\text{high}})$  and  $(t_{\text{high}/2}, -B_{\text{high}})$ .<sup>[34]</sup> As a result, the effect of Zeeman interaction is refocused while  $J$ -coupling evolution is not: the polarization transfer at  $B_{\text{high}}$  continues while fast oscillations will not cause problems for the experimental settings. This refocused type of alt-SABRE-SHEATH similar to refocused INEPT (INEPT+) we suggest calling alt-SABRE-SHEATH+.

The oscillations of  $^1\text{H}/^{15}\text{N}$  amplitude at  $B_{\text{low}}$  with frequency  $\nu$  (close to LAC condition) and at  $B_{\text{high}}$  with frequency  $\nu_{\text{H}} + |\nu_{^{15}\text{N}}|$  (weak  $^1\text{H}-^{15}\text{N}$  coupling) were uncovered experimentally and confirmed by simulations. For  $t_{\text{low}}, t_{\text{high}}$  shorter than  $1/J_{\text{HN}}$  we showed that a higher polarization than for common SABRE-SHEATH can be achieved. Since we only assessed a narrow parameter space further investigations may provide yet higher polarization. The presented simulations and experiments were focused on  $^{15}\text{N}$  of acetonitrile. If and to what extend the polarization of other nuclei and other substrates can be boosted has to be investigated, too. Still, we expect that this approach will allow to enhance the signal of many other SABRE substrates.

## Methods

**SABRE-SHEATH** (Figure 1a, SI, Figure S1–S3).  $B_{\text{hyp}}$  was varied in the range of  $-0.5$  to  $3.5 \mu\text{T}$  to find  $B_{\text{LAC}}$ .  $\text{pH}_2$  was flushed continuously. Close to 100% enrichment  $\text{pH}_2$  was prepared using in house built liquid helium  $\text{pH}_2$  generator.<sup>[30]</sup>

**Alt-SABRE-SHEATH** (Figure 3 and 4, SI, Figure S4–S8). Alt-SABRE-SHEATH sequence (Figure 1b) has four experimental parameters, which were varied:  $t_{\text{low}}, t_{\text{high}}, B_{\text{low}}$  and  $B_{\text{high}}$ . Ramp time  $t_{\text{ramp}}$  was kept constant and equal to 10 ms. The alt-SABRE cycle was repeated  $n$ -times to reach a constant hyperpolarization time. Then a  $90^\circ$  RF-pulse flipped the  $^{15}\text{N}$  and  $^1\text{H}$  spins into the transversal plane for NMR signal observation. Since a broad band SQUID based detector was used, the  $^{15}\text{N}$  and  $^1\text{H}$  signals are read out simultaneously. Parahydrogen was bubbled through the reactor during the entire experiment. Since the variation of all parameters is very time consuming due to a long hyperpolarization period  $t_{\text{hyp}} > 10$  s only some projections of this 4-dimensional experimental space were measured (Figure 3 and 4, SI, Figure S4–S8). The alternating magnetic fields were created by a homemade current source that was controlled by an arbitrary waveform generator (model Rohde & Schwarz HM8150).

**Sample preparation.** The samples consisted of  $40 \mu\text{L}$  acetonitrile- $^{15}\text{N}$  (98%  $^{15}\text{N}$ , Merck, CAS: 14149–39-4) and 3 mg  $[\text{Ir}(\text{MesCODCI})]^{[23]}$  (in house synthesis) catalyst dissolved in 14 mL methanol- $\text{H}_4$  (99% purity). The sample was conducted into a

2 mL reactor. Due to constant  $\text{pH}_2$  bubbling the sample evaporated at a rate of  $\approx 1$  mL/h enabling a maximum measurement time of  $\approx 10$  h (signal stability, SI, Figure S3).

**ULF MRI setup.** The home-made ULF MRI setup consists of a broad band SQUID based detector, sitting inside a low noise fiberglass dewar.<sup>[35]</sup> A homogenous magnetic field is achieved by using a tetracoil with a sphere radius of 260 mm. A Helmholtz coil accomplishes RF transmission and spin rotation. The whole system sits inside a cubic shielding chamber consisting of two layers of  $\mu$ -metal for shielding low frequency magnetic fields and one aluminum layer for shielding RF fields.

The volume of the hyperpolarization reactor is about 2 mL. It has an inlet for the  $\text{pH}_2$  and in- and outlets to the adjacent reservoir. As soon as the sample level in the reactor decreases, new sample from the reservoir flows into the reaction chamber.<sup>[30]</sup>

**SABRE simulations.** SABRE experiments were simulated using the MOIN spin library<sup>[36]</sup> and the quantitative SABRE theory.<sup>[19]</sup> The effective association and dissociation exchange constants for the substrate were  $k_{\text{a}}' = 2 \text{ s}^{-1}$ ,  $k_{\text{d}} = 20 \text{ s}^{-1}$ . The parameters of  $[\text{IrH}_2(\text{S} = ^{15}\text{N})_2] = \text{AA}'\text{XX}'$ : high-field  $T_1$  of  $^1\text{H}$  was 1 s for  $^1\text{H}$  and 6 s for  $^{15}\text{N}$ . Their respective chemical shifts were  $-22$  ppm and 0 ppm.  $J$ -coupling constants were  $^2J_{\text{HN}}^{\text{trans}} = -24$  Hz,  $^2J_{\text{HN}}^{\text{cis}} = 0$  and  $^2J_{\text{HH}} = -8$  Hz. The parameters of free substrate ( $^{15}\text{N}$ ) were: high field  $T_1 = 60$  s and chemical shift 100 ppm.

## Author Contributions

KB, ANP, NK: conceptualization, methodology, writing – original draft, preparation. KB, ANP, NK, MP: investigation. MP:  $[\text{Ir}]$  synthesis. KB, NK: experiments. ANP: simulations. KS, JB, JBH: supervision. KS, JBH, ANP: funding acquisition. KS, JB: provided the environment. All authors contributed to discussions, writing and helped interpreting the results and have given approval to the final version of the manuscript.

## Acknowledgements

We acknowledge funding from German Federal Ministry of Education and Research (BMBF) within the framework of the e: Med research and funding concept (01ZX1915 C), DFG (HO-4602/2-2, HO-4602/3, GRK2154-2019, EXC2167, FOR5042, TRR287), Kiel University and the Faculty of Medicine. MOIN CC was funded by a grant from the European Regional Development Fund (ERDF) and the Zukunftsprogramm Wirtschaft of Schleswig-Holstein (Project no. 122-09-053). Open Access funding enabled and organized by Projekt DEAL.

## Conflict of Interest

The authors declare no conflict of interest.

**Keywords:** alt SABRE SHEATH · p<sub>H</sub><sub>2</sub> hyperpolarization · parahydrogen · level anti-crossing · acetonitrile

- [1] K. H. Mok, P. J. Hore, *Methods* **2004**, *34*, 75–87.
- [2] N. Eshuis, N. Hermkens, B. J. A. Van Weerdenburg, M. C. Feiters, F. P. J. T. Rutjes, S. S. Wijmenga, M. Tessari, *J. Am. Chem. Soc.* **2014**, *136*, 2695–2698.
- [3] K. V. Kovtunov, O. G. Salnikov, V. V. Zhivonitko, I. V. Skovpin, V. I. Bukhtiyarov, I. V. Koptuyug, *Top. Catal.* **2016**, *59*, 1686–1699.
- [4] T. Kress, A. Walrant, G. Bodenhausen, D. Kurzbach, *J. Phys. Chem. Lett.* **2019**, *10*, 1523–1529.
- [5] J. T. Grist, M. Chen, G. J. Collier, B. Raman, G. Abu Eid, A. McIntyre, V. Matthews, E. Fraser, L.-P. Ho, J. M. Wild, F. Gleeson, *Radiology* **2021**.
- [6] S. J. Nelson, J. Kurhanewicz, D. B. Vigneron, P. E. Z. Larson, A. L. Harzstark, M. Ferrone, M. Van Criekinge, J. W. Chang, R. Bok, I. Park, G. Reed, L. Carvajal, E. J. Small, P. Munster, V. K. Weinberg, J. H. Ardenkjær-Larsen, A. P. Chen, R. E. Hurd, L. I. Odegardstuen, F. J. Robb, J. Tropp, J. A. Murray, *Sci. Transl. Med.* **2013**, *5*, 198ra108.
- [7] N. Chattergoon, F. Martínez-Santesteban, W. B. Handler, J. H. Ardenkjær-Larsen, T. J. Scholl, *Contrast Media Mol. Imaging* **2013**, *8*, 57–62.
- [8] C. H. Cunningham, J. Y. C. Lau, A. P. Chen, B. J. Geraghty, W. J. Perks, I. Roifman, G. A. Wright, K. A. Connelly, *Circ. Res.* **2016**, *119*, 1177–1182.
- [9] N. Amor, P. P. Zänker, P. Blümler, F. M. Meise, L. M. Schreiber, A. Scholz, J. Schmiedeskamp, H. W. Spiess, K. Münnemann, *J. Magn. Reson.* **2009**, *201*, 93–99.
- [10] J. B. Hövener, N. Schwaderlapp, T. Lickert, S. B. Duckett, R. E. Mewis, L. A. R. Highton, S. M. Kenny, G. G. R. Green, D. Leibfritz, J. G. Korvink, J. Hennig, D. Von Elverfeldt, *Nat. Commun.* **2013**, *4*, 2946.
- [11] A. N. Pravdivtsev, A. V. Yurkovskaya, H. M. Vieth, K. L. Ivanov, *J. Phys. Chem. B* **2015**, *119*, 13619–13629.
- [12] O. Semenova, P. M. Richardson, A. J. Parrott, A. Nordon, M. E. Halse, S. B. Duckett, *Anal. Chem.* **2019**, *91*, 6695–6701.
- [13] F. Ellermann, A. Pravdivtsev, J.-B. Hövener, *Magn. Reson.* **2021**, *2*, 49–62.
- [14] S. Korchak, S. Mamone, S. Glöggler, *ChemistryOpen* **2018**, *7*, 672–676.
- [15] J. F. P. Colell, A. W. J. Logan, Z. Zhou, R. V. Shchepin, D. A. Barskiy, G. X. Ortiz, Q. Wang, S. J. Malcolmson, E. Y. Chekmenev, W. S. Warren, T. Theis, *J. Phys. Chem. C* **2017**, *121*, 6626–6634.
- [16] R. W. Adams, J. A. Aguilar, K. D. Atkinson, M. J. Cowley, P. I. P. Elliott, S. B. Duckett, G. G. R. Green, I. G. Khazal, J. Lopez-Serrano, D. C. Williamson, *Science* **2009**, *323*, 1708–1711.
- [17] A. N. Pravdivtsev, A. V. Yurkovskaya, H. Zimmermann, H. M. Vieth, K. L. Ivanov, *Chem. Phys. Lett.* **2016**, *661*, 77–82.
- [18] A. N. Pravdivtsev, A. V. Yurkovskaya, H. M. Vieth, K. L. Ivanov, R. Kaptein, *ChemPhysChem* **2013**, *14*, 3327–3331.
- [19] S. Knecht, A. N. Pravdivtsev, J. B. Hövener, A. V. Yurkovskaya, K. L. Ivanov, *RSC Adv.* **2016**, *6*, 24470–24477.
- [20] K. L. Ivanov, A. N. Pravdivtsev, A. V. Yurkovskaya, H. M. Vieth, R. Kaptein, *Prog. Nucl. Magn. Reson. Spectrosc.* **2014**, *81*, 1–36.
- [21] M. L. Truong, T. Theis, A. M. Coffey, R. V. Shchepin, K. W. Waddell, F. Shi, B. M. Goodson, W. S. Warren, E. Y. Chekmenev, *J. Phys. Chem. C* **2015**, *119*, 8786–8797.
- [22] J. R. Lindale, S. L. Eriksson, C. P. N. Tanner, Z. Zhou, J. F. P. Colell, G. Zhang, J. Bae, E. Y. Chekmenev, T. Theis, W. S. Warren, *Nat. Commun.* **2019**, *10*, 395.
- [23] M. J. Cowley, R. W. Adams, K. D. Atkinson, M. C. R. Cockett, S. B. Duckett, G. G. R. Green, J. A. B. Lohman, R. Kerssebaum, D. Kilgour, R. E. Mewis, *J. Am. Chem. Soc.* **2011**, *133*, 6134–6137.
- [24] A. N. Pravdivtsev, J. B. Hövener, *Phys. Chem. Chem. Phys.* **2020**, *22*, 8963–8972.
- [25] D. A. Barskiy, A. N. Pravdivtsev, K. L. Ivanov, K. V. Kovtunov, I. V. Koptuyug, *Phys. Chem. Chem. Phys.* **2016**, *18*, 89–93.
- [26] D. A. Barskiy, S. Knecht, A. V. Yurkovskaya, K. L. Ivanov, *Prog. Nucl. Magn. Reson. Spectrosc.* **2019**, *114–115*, 33–70.
- [27] A. N. Pravdivtsev, K. L. Ivanov, A. V. Yurkovskaya, P. A. Petrov, H. H. Limbach, R. Kaptein, H. M. Vieth, *J. Magn. Reson.* **2015**, *261*, 73–82.
- [28] J. Eills, J. W. Blanchard, T. Wu, C. Bengs, J. Hollenbach, D. Budker, M. H. Levitt, *J. Chem. Phys.* **2019**, *150*, 174202.
- [29] J. R. Lindale, S. L. Eriksson, C. P. N. Tanner, W. S. Warren, *Sci. Adv.* **2020**, *6*, eabb6874.
- [30] K. Buckenmaier, M. Rudolph, P. Fehling, T. Steffen, C. Back, R. Bernard, R. Pohmann, J. Bernarding, R. Kleiner, D. Koelle, M. Plaumann, K. Scheffler, *Rev Sci Instrum* **2018**, *89*, 125103.
- [31] K. Buckenmaier, K. Scheffler, M. Plaumann, P. Fehling, J. Bernarding, M. Rudolph, C. Back, D. Koelle, R. Kleiner, J. B. Hövener, A. N. Pravdivtsev, *ChemPhysChem* **2019**, *20*, 2823–2829.
- [32] E. Cavallari, C. Carrera, T. Boi, S. Aime, F. Reineri, *J. Phys. Chem. B* **2015**, *119*, 10035–10041.
- [33] A. N. Pravdivtsev, A. V. Yurkovskaya, N. N. Lukzen, K. L. Ivanov, H. M. Vieth, *J. Phys. Chem. Lett.* **2014**, *5*, 3421–3426.
- [34] S. L. Eriksson, J. R. Lindale, X. Li, W. S. Warren, *arXiv.org* **2021**, arXiv:2107.04687.
- [35] H. C. Seton, J. M. S. Hutchison, D. M. Bussell, *Cryogenics (Guildf.)* **2005**, *45*, 348–355.
- [36] A. N. Pravdivtsev, J. B. Hövener, *Chem. A Eur. J.* **2019**, *25*, 7580–7580.

Manuscript received: July 20, 2021

Revised manuscript received: September 16, 2021

Accepted manuscript online: September 21, 2021

Version of record online: October 14, 2021